Structural, vibrational, and thermodynamic properties of Al-Sc alloys and intermetallic compounds

M. Asta
Department of Materials Science and Engineering, Northwestern University, Evanston, Illinois 60208-3108

V. Ozoliņš
Sandia National Laboratories, MS 9161, P.O. Box 969, Livermore, California 94551-0969

(Received 24 January 2001; published 7 August 2001)

We present results of a theoretical study of the temperature-dependent structural and thermodynamic properties of solid-phase Al-Sc alloys and compounds based upon first-principles calculations of electronic free energies and ionic vibrational spectra. This work extends a previous first-principles study of the fcc portion of the Al-Sc phase diagram which demonstrated a large effect of vibrational free energy upon calculated Sc solid-solubility limits [V. Ozoliņš and M. Asta, Phys. Rev. Lett. **86**, 448 (2001)]. Here the contributions of nonconfigurational (electronic and vibrational) entropies to the free energies of solid-phase Al-Sc alloys and compounds are analyzed in further detail, and the accuracy of the approximations employed in these calculations is assessed. For each of the reported intermetallic compounds in this system, calculated formation enthalpies agree to within 10% (0.05 eV/atom) of published calorimetry measurements. Large negative entropies of formation, equal to $-0.77k_B$/atom, $-0.58k_B$/atom, and $-0.24k_B$/atom are calculated for cubic Al_3Sc, cubic AlSc, and orthorhombic AlSc compounds, respectively, resulting primarily from the stiffening of nearest-neighbor Al-Sc bonds in the intermetallic phases relative to elemental Al and Sc. The net effects of nonconfigurational free energy contributions to the fcc portion of the Al-Sc phase diagram are 100 and 450 K decreases in the calculated Al solvus phase boundary temperatures associated with electronic and vibrational entropy, respectively, at the maximum measured Sc solid-solubility limit.

DOI: 10.1103/PhysRevB.64.094104 PACS number(s): 64.70.Kb, 63.20.−e, 64.75.+g, 65.20.+w

I. INTRODUCTION

Al-rich Al-Sc alloys have received growing attention as high-specific-strength materials. Sc is known to give rise to the highest increase in strength, per atomic percent, of any alloying addition in Al,[1] and it is only slightly more dense (about 11%) than Al itself. The strengthening effect of Sc in Al is attributed to the formation of small (20–30 nm) coherent Al_3Sc precipitates which form homogeneously during the aging of supersaturated Al(Sc) solid solutions[1,2] in the temperature range of 300–350 °C. In contrast to many commercial Al alloys, the strengthening precipitate phase in Al-Sc is thermodynamically stable to temperatures well above the melting point of Al. The Al_3Sc phase forms in the fcc-based $L1_2$ (Cu_3Au prototype) crystal structure and undergoes incongruent melting at a peritectic temperature of 1300 °C.[3,4]

Despite the growing interest in Al(Sc) alloys, uncertainties persist related to the Al-Sc phase diagram. For example, the crystal structure of the equiatomic AlSc phase remains uncertain, with both $B2$ (CsCl prototype) and B_f (BCr prototype) structures having been reported in the literature.[5,6] Recently, two assessments of the Al-Sc phase diagram have been published by Murray[3] and Cacciamani *et al.*[4] The optimized thermodynamic parameters obtained in these two assessments show significant differences, as do the calculated phase boundaries for near-equiatomic alloy compositions. At present, ternary additions to Al-Sc alloys are being investigated in the development of high-specific-strength materials for potential applications at high homologous temperatures. As a basis for modeling phase stability in these multicomponent systems, an improved understanding of the binary Al-Sc phase diagram is desirable.

In the present work the structural and thermodynamic properties of Al-Sc compounds and the Al-rich solid-solution phase have been studied from first principles based upon electronic-structure calculations of total energies and ionic vibrational spectra. First-principles methods have seen wide application in the study of alloy phase stability and the calculation of composition-temperature phase diagrams, as reviewed by de Fontaine,[7] Ducastelle,[8] and Zunger.[9] The limited accuracy of the thermodynamic properties obtained in these calculations has limited severely their application in the process of alloy development.[10] Recently we have found that the accuracy of first-principles-calculated phase boundaries for dilute Al(Sc) alloys is greatly improved through the incorporation of vibrational contributions to alloy free energies.[11] Such contributions are typically either neglected in first-principles calculations of substitutional alloy phase diagrams or incorporated based upon approximate models. In our previous work harmonic ionic vibrational entropy, computed from first-principles linear-response[12] calculations of dynamical matrices, was found to account for a factor of 27 increase in calculated solid-solubility limits for Sc in Al, leading to a 450 K decrease in the calculated phase-boundary temperature at the maximum solubility concentration and agreement to within 50 K of experimentally measured phase boundaries.

In the present paper we extend our initial work, presenting a further analysis of the magnitude of nonconfigurational contributions to the thermodynamic properties of the Al-rich solid solution as well as Al_3Sc and AlSc intermetallic com-

pounds. To gauge the accuracy of the approximations employed in the first-principles computations, we also present comparisons between our calculations and available experimental data. At present a limited number of first-principles studies of the vibrational properties of intermetallic compounds have been published, and relatively little information is available concerning the magnitudes and microscopic origins of vibrational entropy in this important class of materials. In the present work we present a detailed analysis of the factors contributing to the large calculated vibrational entropies of formation of Al-Sc compounds.

II. METHODOLOGY

A. Electronic structure and phonon spectra

The structural and thermodynamic properties of Al-Sc intermetallic compounds and Al-rich solid solutions have been studied based upon *ab initio* calculations of total energies and ionic vibrational spectra. These calculations employed two related approaches based upon electronic density-functional theory in the local-density approximation (LDA) (Ref. 13) as described below.

Structural and energetic properties have been computed using the *ab initio* total-energy and molecular-dynamics program VASP (Vienna *ab initio* simulation package) developed at the Institut für Material-physik of the Universität Wien.[14–16] The VASP code makes use of ultrasoft pseudopotentials[17] and an expansion of the electronic wave functions in plane waves. The Sc pseudopotential was constructed to treat $3p$ states as valence, since these states are fairly extended and have been found to affect calculated equilibrium lattice parameters and defect energies. For all of the VASP results presented below use was made of a plane-wave cutoff of 223.3 eV. In the calculations of formation energies, electronic entropy, and structural properties for Al-Sc intermetallic compounds, use was made of ''special'' reciprocal-space **k** points[18] generated from the following meshes: $16\times16\times16$ for fcc Al, $16\times16\times16$ for $L1_2$ Al_3Sc, $6\times6\times6$ for Al_2Sc, $20\times20\times20$ for $B2$ AlSc, $20\times8\times12$ for B_f AlSc, $12\times12\times9$ for $AlSc_2$, and $18\times18\times12$ for hcp Sc. Based upon test calculations for Al-Sc compounds performed with differing **k**-point meshes and plane-wave cutoffs, formation energies are estimated to be converged to within a few meV/atom, lattice parameters to within a fraction of a percent, and electronic formation entropies to within $0.02k_B$/atom. Electronic densities of states (DOS) were calculated using the linear tetrahedron method.

Harmonic vibrational spectra were computed using the density-functional linear-response method.[12] Our implementation of this powerful approach employs norm-conserving pseudopotentials (NCPPs) specifically optimized for use with a plane-wave basis set.[19] The optimization procedure enables efficient calculations for transition-metal atoms with localized d orbitals, ensuring that calculated structural and vibrational properties converge rapidly with respect to the plane-wave energy cutoff used to represent electronic wave functions. Scandium $3s$ and $3p$ states were treated as valence (see previous paragraph), and the nonlinear core correction[20] was used for Al to account for the effect of core charge density on electronic exchange-correlation effects. The plane-wave cutoff energy was set to 544.2 eV, since test calculations showed that further increase in the size of the basis set changed the calculated phonon frequencies by at most a couple of percent. Electronic states were sampled on regular **k**-point grids to ensure convergence of the calculated phonon frequencies to within 0.05 THz. This required a $12\times12\times12$ regular mesh for Al_3Sc, $16\times16\times16$ for the cubic $B2$ AlSc compound, and $8\times12\times16$ for the orthorombic B_f structure of AlSc. Dynamical matrices were calculated on regular grids of phonon wave vectors **q** and then Fourier transformed to real space to yield real-space interatomic force constants. These force constants were subsequently used to interpolate phonon dispersions to arbitrary wave vectors **q** and to calculate accurate vibrational entropies and the phonon DOS. The contribution of each phonon mode to the phonon DOS was represented by a Gaussian with a width of 0.15 THz. Use was made of regular phonon wave-vector meshes of $4\times3\times4$, $8\times8\times8$, and $6\times6\times6$ for B_f-type AlSc, $B2$ AlSc, and Al_3Sc compounds, respectively. Phonon-mode Grüneisen parameters were calculated by taking finite differences between phonon frequencies at two volumes separated by $\approx4\%$.

A different approach was adopted for calculating excess energies and entropies of Sc impurities in fcc Al matrix. Since the latter calculations involve very large unit cells (up to 216 atoms), it is impractical to achieve absolute convergence with respect to the number of reciprocal-space points used in the sampling of electron and phonon states. Instead, we adopted the equivalent **k**-point method proposed by Froyen,[21] which ensures strict equivalence of **k**-point grids used in supercell and one-atom-per-cell fcc Al calculations. The basic idea of Froyen's method is that numerical errors in the properties of fcc Al will cancel out between the two sets of calculations, leaving one with the intrinsic effect of a Sc impurity. This approach is widely used and has been shown to lead to rapid convergence on meshes much coarser than ones employed in the present study.[22] Further details of the electronic-structure supercell calculations are given below. For sampling phonon modes (for example, in the calculation of impurity vibrational free energies) use was made of a $3\times3\times3$ mesh for 27-atom supercells, while one symmetry-inequivalent special point was employed for 64-atom cells.

B. Electronic free energy

Electronic entropy and free energy are evaluated in the independent electron approximation using eletronic-state occupation numbers given by the Fermi-Dirac distribution function $f(\epsilon,T)$ (Ref. 23):

$$S_{\mathrm{el}}(T)=-k_B\sum_{\mathbf{k}n}\{f(\epsilon_{\mathbf{k}n},T)\ln f(\epsilon_{\mathbf{k}n},T)+[1-f(\epsilon_{\mathbf{k}n},T)]\ln[1-f(\epsilon_{\mathbf{k}n},T)]\}. \quad (1)$$

Many-body electronic correlation effects beyond those of the homogeneous electron gas are excluded due to the approxi-

mate nature of the LDA functional. In the vast majority of cases, $S_{\mathrm{el}}(T)$ is a linear function of T at temperatures below the Fermi energy:

$$S_{\mathrm{el}} = C_{\mathrm{el}} T + O\left[\left(\frac{k_B T}{\epsilon_F}\right)^2\right], \tag{2}$$

where C_{el} is the linear coefficient of the low-temperature heat capacity neglecting the effective mass enhancement factor $(1+\lambda)$ due to electron-phonon interactions. While the entropy is a linear function of T, the electronic energy E_{el} and electronic free energy $G_{\mathrm{el}} = E_{\mathrm{el}} - TS_{\mathrm{el}}$ are quadratic functions of temperature:[23]

$$E_{\mathrm{el}} = E_0 + \frac{1}{2} C_{\mathrm{el}} T^2 + O\left[\left(\frac{k_B T}{\epsilon_F}\right)^3\right], \tag{3}$$

$$G_{\mathrm{el}} = G_0 - \frac{1}{2} C_{\mathrm{el}} T^2 + O\left[\left(\frac{k_B T}{\epsilon_F}\right)^3\right]. \tag{4}$$

Equations (2)–(4) are applicable to nonmagnetic systems that do not exhibit electronic topological transitions or other electronic-structure-related anomalies.

For the purpose of computing Al-Sc alloy phase boundaries values of the electronic free energy are required as a function of temperature. In practice, the electronic free energy G_{el} was calculated self-consistently at three different temperatures $k_B T = 40$, 60, and 80 meV and subsequently fit to the functional forms provided by Eqs. (2)–(4). The accuracy of the fit over the temperature range of interest was estimated to be better than 20 meV/atom (2.5%) for the quantity $4\Delta G_{\mathrm{el}}^{\alpha'} - \Delta G_{\mathrm{el}}^{\mathrm{Sc}}$ which arises in an exponentional equation for the Sc solubility limit, as described below. Special care was taken in evaluating the reciprocal-space sums involved in Eq. (1), since the electronic free energy of fcc Al converges rather slowly with respect to the number of special **k** points. As explained in the previous section, to facilitate convergence of the values of the electronic free energy of formation, use was made of the equivalent **k**-point scheme of Froyen.[21]

C. Vibrational free energy

This section summarizes the key expressions describing vibrational free energies and temperature-dependent structural properties. The entropy associated with harmonic ionic vibrations at high temperatures is proportional to the logarithmic moment of the vibrational DOS, $g(\omega)$ (Ref. 23):

$$S_{\mathrm{vib}} = k_B \int [1 + \ln(k_B T/\hbar\omega) + \cdots] g(\omega) d\omega. \tag{5}$$

Higher-order terms in Eq. (5) are negligibly small for $k_B T > \hbar\langle\omega\rangle$, i.e., for temperatures higher than the characteristic Debye temperature θ_D of ionic vibrations. For typical metals θ_D is well below room temperature, and Eq. (5) can be truncated after the first two terms. Using Eq. (5), one obtains that the formation entropy ΔS_{vib} is determined by the difference in vibrational DOS between the compound and its composition-weighted constituents, $\Delta g(\omega) = g(\omega) - (1-c) g_{\mathrm{Al}}(\omega) - c g_{\mathrm{Sc}}(\omega)$, where $g_{\mathrm{Al}}(\omega)$ and $g_{\mathrm{Sc}}(\omega)$ are vibrational DOS of Al and Sc, respectively. For ΔS_{vib} one obtains that the latter is proportional to the logarithmic moment of $\Delta g(\omega)$:

$$\Delta S_{\mathrm{vib}} = k_B \int \ln(k_B T/\hbar\omega) \Delta g(\omega) d\omega. \tag{6}$$

Using Eq. (6) and the fact that $\int \Delta g(\omega) d\omega = 0$, one finds that the harmonic vibrational entropy of formation approaches a constant value at high temperatures. The vibrational free energy of formation in the harmonic approximation is thus a linear function of temperature:

$$\Delta G_{\mathrm{vib}} = -T \Delta S_{\mathrm{vib}}. \tag{7}$$

Anharmonic effects (e.g., thermal expansion) lead to a temperature dependence of the vibrational entropies of formation. Thermal expansion has been estimated using the quasiharmonic approximation.[24] The quasiharmonic approximation has been shown to accurately reproduce measured thermal expansion coefficients in metals and to lead to an accurate description of bulk free energies in metals up to high homologous temperatures.[25,26] Volume-dependent, quasiharmonic vibrational free energies were derived from the calculated phonon-mode Grüneisen parameters $\gamma_{\mathbf{q}n} = d \ln \omega_{\mathbf{q}n} / d \ln V$. The coefficient of linear thermal expansion is given by the formula (the following formulas are strictly valid only for cubic compounds)

$$\alpha_L(T) = \frac{C_V(T)\gamma_G(T)}{3 V_0 B_0}, \tag{8}$$

where V_0 is the equilibrium volume at $T = 0$ K and B_0 is the isothermal bulk modulus. $C_V(T)$ is the temperature-dependent heat capacity at constant volume:

$$C_V(T) = \frac{1}{N} \sum_{\mathbf{q}n} C\left(\frac{\hbar\omega_{\mathbf{q}n}}{k_B T}\right). \tag{9}$$

Here N is the total number of atoms and $C(x)$ is the constant-volume heat capacity function:

$$C(x) = \frac{k_B x^2}{4 \sinh^2(x/2)}. \tag{10}$$

It is evident from Eqs. (9) and (10) that a phonon mode contributes appreciably to the heat capacity only when its energy is comparable to $k_B T$ and its contribution approaches the value k_B when $k_B T \gg \hbar\omega$. The Grüneisen parameter $\gamma_G(T)$ is expressed as

$$\gamma_G(T) = \frac{1}{N C_V(T)} \sum_{\mathbf{q}n} \gamma_{\mathbf{q}n} C\left(\frac{\hbar\omega_{\mathbf{q}n}}{k_B T}\right). \tag{11}$$

From the properties of $C(x)$ it follows that the Grüneisen parameter $\gamma_G(T)$ approaches a constant value $\bar{\gamma}$ at high temperature. Together with the fact that the heat capacity tends to the Dulong-Petit limit of $3k_B$ per atom, the coefficient of linear thermal expansion approaches a constant value α_L

TABLE I. Calculated and measured properties for $L1_2$ Al_3Sc. V_0 represents the atomic volume, ΔH the formation enthalpy, and B_0 the bulk modulus.

	V_0 (Å^3/atom)	ΔH (eV/atom)	B_0 (Mbar)
NCPP[a]	16.1	−0.523	0.96
VASP[b]	16.5	−0.497	0.94
FLAPW[c]	16.4	−0.537	0.96
FLAPW[d]	16.5	−0.498	0.92
LMTO-ASA[e]	16.7	−0.446	0.93
Expt.	17.24-17.29[f]	−0.451[g]	0.92[h], 0.99[i]

[a]Present study, norm-conserving pseudopotential results.
[b]Present study, ultrasoft pseudopotential results.
[c]Reference 30.
[d]Reference 31.
[e]Reference 32.
[f]Reference 27.
[g]Reference 4.
[h]Reference 28.
[i]Reference 29.

$=k_B\overline{\gamma}/V_0B_0$ above the Debye temperature, where $\overline{\gamma}$ is the Grüneisen parameter averaged over all phonon modes. However, $\alpha_L(T)$ can show significant temperature dependence at and below the Debye temperature due to the T dependence of both $C_V(T)$ and $\gamma_G(T)$.

The rate of the vibrational entropy increase due to thermal expansion is

$$\left(\frac{\partial S}{\partial V}\right)_T\left(\frac{\partial V}{\partial T}\right)_P = 3\alpha_L\gamma_G C_V. \quad (12)$$

This increase in entropy is partly offset by the increase in the static total energy term due to volume expansion. The net effect of thermal expansion on the vibrational free energy is only half of that given by Eq. (12):

$$\Delta' G_{\rm vib} = -\frac{3}{2}\int_0^T \alpha_L(T')\gamma_G(T')C_V(T')T'dT', \quad (13)$$

which has to be added to the harmonic entropy of formation given by Eq. (7). The integral in Eq. (13) can be split into two contributions. At and above the Debye temperature where $\alpha_L(T)$, $\gamma_G(T)$, and $C_V(T)$ are constant, we find that a temperature increase ΔT will lead to a $\Delta' G_{\rm vib} = -9[\overline{\gamma}k_B\Delta T]^2/(2V_0B_0)$ decrease in the quasiharmonic free energy due to thermal expansion. At low temperatures both $\alpha_L(T)$ and $C_V(T)$ are small; hence, the contribution to integral in Eq. (13) is also quite small and usually can be neglected in comparison with the $T>\theta_D$ contribution.

III. RESULTS

A. Structural and thermodynamic properties at $T=0$ K

For the Al_3Sc phase we list in Table I values of the zero-temperature formation enthalpy (ΔH), atomic volume (V_0), and bulk modulus (B_0) obtained from the present calculations, using the two pseudopotential-based approaches described above. These values are compared with experimental data[4,27–29] as well as previously published first-principles results.[30–32] We note a satisfactory level of agreeement between the present pseudopotential results and previously published all-electron calculations based upon the full-potential linear augmented plane-wave method (FLAPW).[33] As is typical for calculations based upon the LDA, the theoretical values for atomic volumes (bulk moduli) are underestimated (overestimated) compared to experimental measurements by roughly 4–6 % (0–6 %). Compared with the VASP results given in Table I, the NCPP calculations give rise to a more strongly bound Al_3Sc compound, with a more negative value of ΔH (by roughly 25 meV/atom), a smaller volume (by 3%), and a larger bulk modulus (by 2%). This same trend is found for $B2$ and B_f AlSc compounds where NCPPs calculated formation enthalpies are more negative by roughly 5%. While the NCPP results given in Table I show slightly larger discrepancies with experimental data (relative to the VASP numbers), these values are closer to the most recent FLAPW values.[30]

In Table II calculated structural and elastic properties are compared with available experimental data[27,34–36] for the elemental constituents and each of the intermetallic compounds reported in Al-Sc system. The experimental lattice parameter data for the intermetallics in this table were taken from the compilation by Villars and Calvert.[27] For the hexagonal $AlSc_2$ compound our calculated value for the lattice parameter ratio c/a is seen to agree very well with experimental measurements. By contrast, for the orthorhombic B_f AlSc compound we find large discrepancies between our results and the unit cell dimensions b/a and c/a reported by Schuster and Bauer,[5] with calculated values being almost twice larger. This result is surprising, as lattice-parameter ratios for metallic structures predicted from LDA-based calculations are generally found to agree to within a few percent of experimental measurements. It is noted in the compilation by Villars and Calvert[27] that the values of b/a and c/a reported by Schuster and Bauer differ substantially from those for all other compounds crystallizing in the BCr structure type, and a "printing error" in the unit cell dimensions is suggested.[27] We note that, consistent with the observation by Villars and Calvert, our calculated structural parameters for the BCr-type AlSc structure are relatively close to those measured for the same structure in the related Al-Y system. Specifically, for B_f AlY measured b/a and c/a ratios are in the ranges 2.9665–2.9966 and 1.1290–1.1357, respectively,[27] whereas our calculated values for AlSc are $b/a=3.34$ and $c/a=1.31$.

In Fig. 1 we present a comparison between calculated and experimentally measured[4,37,38] enthalpies of formation (ΔH) for Al-Sc intermetallic compounds. The dark solid symbols in Fig. 1 represent the results of the present first-principles calculations at zero temperature. Shaded symbols in Fig. 1 correspond to measured data from high-temperature[37,38] (diamonds) and reaction-drop[4] (circles) calorimetry.[39] The open symbols in Figs. 1 and 2 correspond to estimates based on two recent assessments of the Al-Sc phase diagram,[3,4] as discussed further below. For each compound the measured and calculated values of ΔH are found to agree to within

TABLE II. Calculated temperature-dependent structural and elastic properties for Al-Sc compounds. V_0 and B_0 denote zero-temperature atomic volumes and bulk moduli, respectively. Calculated high-temperature coefficients of volume thermal expansion $\alpha_V = 3\alpha_L = (1/V) \times (\partial V/\partial T)_p$ and the temperature derivative of the bulk modulus $(\partial B/\partial T)_p$ are given in the final two columns. Experimental values of lattice parameters at room temperature are given in parentheses and are taken from the compilation of Villars and Calvert (Ref. 27) for the intermetallic compounds and from Ref. 35 for elemental Al and Sc. The experimental values for the volume thermal expansion coefficients of Al_3Sc and elemental metals are from Refs. 36 and 34, respectively. Except where indicated, calculated lattice parameters and atomic volume numbers were obtained using VASP, and thermal properties [α_V and $(\partial B/\partial T)_p$] are computed by NCPP linear response.

Composition	Structure	V_0 (Å^3/atom)	b/a	c/a	B_0 (Mbar)	α_V (10^{-6} K^{-1})	$(\partial B/\partial T)_p$ (MPa K^{-1})
Al	$A1$(Cu)	15.8	–	–	0.81	66	
		15.7[a]	–	–	0.83		
		16.0[b]	–	–			
		(16.6)				(69)	
Al_3Sc	$L1_2$ (Cu_3Au)	16.5	–	–	0.94	43	−17
		16.1[a]	–	–	0.96		
		16.4[b]	–	–			
		(17.3, 17.29, 17.24)				(22)	
Al_2Sc	$C15$ (Cu_2Mg)	17.3	–	–	0.94		
		(18.15, 18.28)					
AlSc	$B2$ (CsCl)	18.3	–	–	0.84	39	−13
		17.8[a]	–	–	0.87		
		18.0[b]	–	–			
		(19.45, 20.52)					
AlSc	B_f (BCr)	19.2	3.34	1.31	0.76		
		18.8[a]					
		(19.449)	(1.9671)	(0.621 54)			
$AlSc_2$	$B8_2$ ($InNi_2$)	20.2	–	1.26	0.75		
		(21.21, 21.27)		(1.263, 1.261)			
Sc	$A3$ (Mg)	23.0	–	1.57	0.60	21	
		22.1[a]	–	1.53	0.61		
		22.35[b]	–				
		(25.0)		(1.59)		(30)	

[a]NCPP values.

[b]NCPP values that include effect of zero-point motion as calculated from the linear response method.

10% (0.05 eV/atom), with the calculated values being more (less) negative for Al-rich (Sc-rich) compositions. The level of agreement between experiment and theory demonstrated in Fig. 1 is comparable to that obtained in previous first-principles studies for the related Al-Zr (Ref. 40) and Al-Ti systems (a review of calculations for Al-Ti is given by Asta *et al.*[41] and Watson and Weinert.[42]) As indicated in Fig. 1, for the equiatomic AlSc compound we have computed formation enthalpies for both the $B2$ and B_f prototype structures reported by Schuster and Bauer[5] and Schob and Parthé,[6] respectively. We find the $B2$ structure to be stable at low temperatures, with a calculated value of ΔH that is 0.07 eV/atom more negative.

B. High-temperature structural and thermodynamic properties of intermetallic compounds

In Fig. 2 solid symbols correspond to calculated entropies of formation (ΔS) for ordered Al_3Sc and AlSc compounds at a temperature of 600 K. The calculated values of ΔS represent a sum of harmonic-vibrational and electronic contributions at 600 K (anharmonic-vibrational contributions, estimated through the quasiharmonic approximation, were found to be small at this temperature). In these calculations we have neglected configurational contributions to the entropies of formation, assuming that the compounds are perfectly ordered at 600 K (in the case of Al_3Sc this assumption is validated by experimental measurements, as discussed below). The electronic contributions to calculated values of ΔS for the Al_3Sc, CsCl-AlSc, and BCr-AlSc compounds are, respectively, $-0.08k_B$/atom, $-0.14k_B$/atom, and $+0.02k_B$/atom. The negative values for Al_3Sc and $B2$ AlSc originate from a reduction in the electronic DOS near the Fermi level for these compounds relative to the compositions-weighted average for the elemental constituents, as shown in Fig. 3. The suppression in the electronic DOS near the Fermi level, often referred to as a ''pseudogap,'' found for the Al_3Sc and $B2$-AlSc compounds has been obtained in electronic-structure calculations for several other stable transition-metal aluminide compounds (e.g., Refs. 32, 43, and 45). The origin of pseudogaps in these systems has been discussed in detail recently by Weinert and

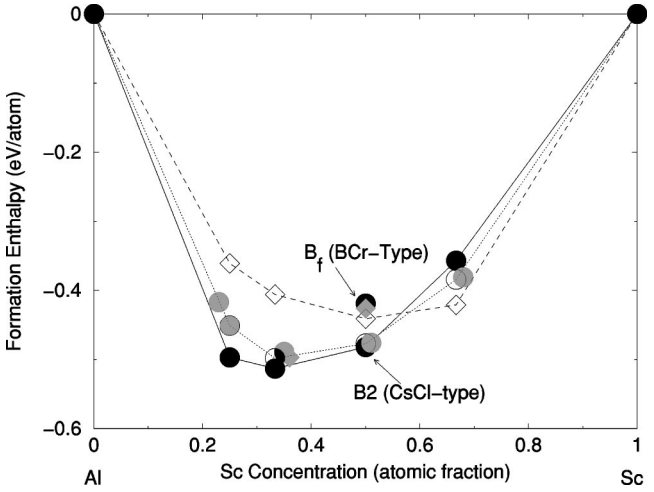

FIG. 1. Enthalpies of formation ΔH are plotted versus Sc composition. Solid symbols are zero-temperature values computed in the present study by VASP. For AlSc we have calculated values of ΔH for both of the reported crystal structures, namely, CsCl and BCr prototypes. The results for CsCl and BCr are the lower and higher values, respectively. Shaded symbols correspond to experimental calorimetry data taken from Jung *et al.* (diamond symbol at composition Al_2Sc) (Ref. 37), Meschel and Kleppa (diamond symbol for AlSc) (Ref. 38), and Cacciamani *et al.* (circles) (Ref. 4). The open symbols give values of ΔH obtained from optimized thermodynamic parameters due to Murray (diamonds) (Ref. 3) and Cacciamani *et al.* (circles) (Ref. 4).

Watson.[45] The electronic DOS plotted for $L1_2$ Al_3Sc in Fig. 3 shows features similar to those for $L1_2$ Al_3Y calculated by Carlsson and Meschter,[43] and the DOS plotted for $B2$ AlSc are similar to that published by Nguyen-Manh and Pettifor.[44]

As compared with the electronic contributions, the calculated *vibrational* formation entropies for Al-Sc intermetallics are found to be substantially larger in magnitude, giving rise

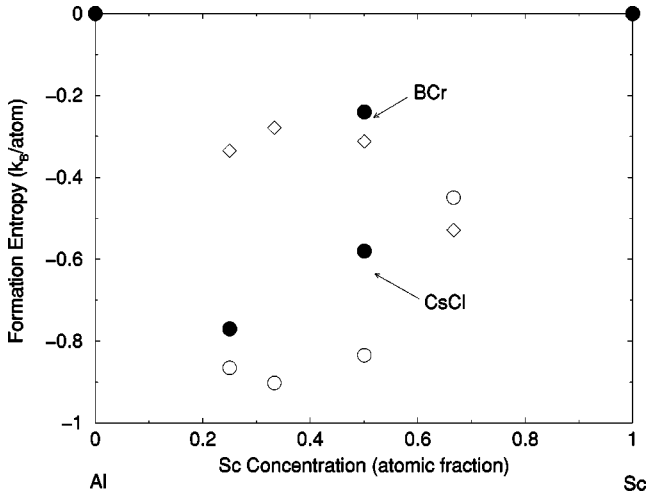

FIG. 2. Entropies of formation ΔS at room temperature are plotted versus Sc composition. Solid circles represent the results of the present first-principles calculations. The open circles and diamonds were obtained from the optimized thermodynamic parameters due to Cacciamani *et al.* (Ref. 4) and Murray (Ref. 3), respectively.

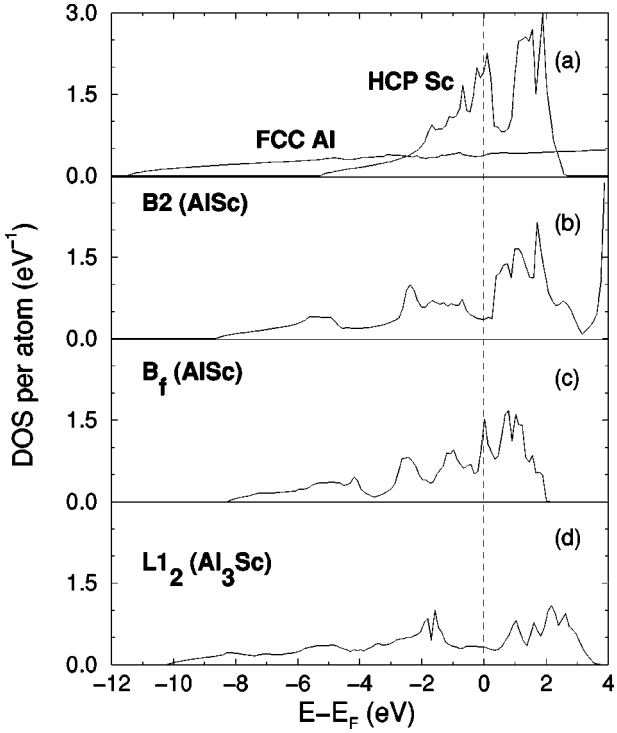

FIG. 3. Electronic densities of states of (a) fcc Al, (b) $B2$ AlSc, (c) B_f AlSc, and (d) $L1_2$ Al_3Sc.

to negative values of ΔS for each of the compounds considered: $-0.70\ k_B$/atom for Al_3Sc, $-0.46\ k_B$/atom for $B2$ Alsc, and $-0.26\ k_B$/atom for B_f AlSc. The origin of the negative vibrational entropies of formation can be understood based upon an analysis of the vibrational DOS. The calculated phonon DOS of fcc Al, hcp Sc, and $L1_2$ Al_3Sc have been published previously in Fig. 2 of Ref. 11. The calculated phonon dispersion curves of cubic $L1_2$ Al_3Sc and $B2$ AlSc compounds, which were not shown in Ref. 11, are given in Figs. 4 and 5, respectively, for future reference and for comparison with experimental data as they become available.

The phonon spectrum of $B2$ AlSc shown in Fig. 5 exhibits two interesting features: (a) low frequencies of the transversal acoustic branch along $[\xi\xi 0]$ with $[\bar{1}10]$ polarization and (b) anomalous longitudinal-mode dispersion along $[\xi\xi\xi]$. The former feature is encountered in many bcc metals and is commonly attributed to small bcc/fcc and bcc/hcp energy differences. It is usually explained by invoking the well-known Bain[46] and Burgers[47] mechanisms for fcc-to-bcc and bcc-to-hcp structural transformations, respectively. The Bain mechanism of bcc-to-fcc transformation involves a homogeneous (100) shear. The energy of this shear is determined by the elastic constant $C'=\frac{1}{2}(C_{11}-C_{12})$, which also determines the acoustic sound velocity and the slope at $\mathbf{q}=0$ for the TA$[\bar{1}10]$ phonon branch. The Burgers bcc-to-hcp mechanism involves a $[\xi\xi 0]$ zone boundary TA$[\bar{1}10]$ phonon combined with a $[110]$ shear. The fcc analog of the $B2$ crystal structure is $L1_0$ (prototype CuAu), and the hcp analog of $B2$ is $B19$ (prototype AuCd). The energies of these structures are calculated to be very close (to within a few

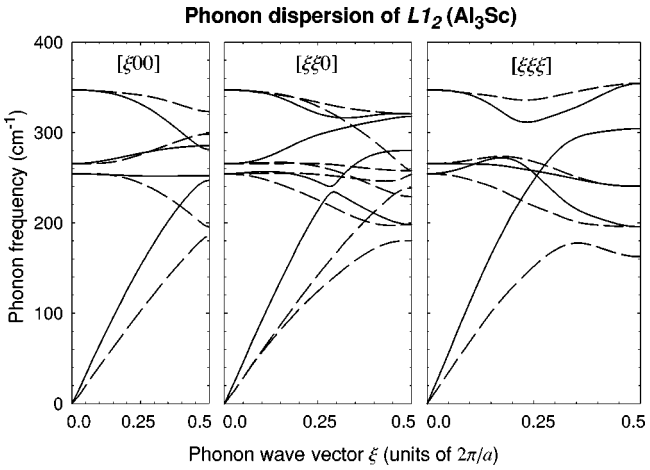

FIG. 4. Phonon dispersion curves of $L1_2$ Al_3Sc. Solid lines show phonon modes for which $q^{-1}\Sigma_i \mathbf{q}\cdot\mathbf{e}_i(\mathbf{q}n)=1$, while dashed lines show modes for which $q^{-1}\Sigma_i \mathbf{q}\cdot\mathbf{e}_i(\mathbf{q}n)=0$. These phonons are true longitidunal and transversal modes when $\mathbf{q}$ is along either the [100] or the [111] direction. For $\mathbf{q}$ along the [110] direction, four modes have polarization vectors directed along [001]. In the remaining eight $[\xi\xi 0]$ modes only the center of mass has to be perpendicular or parallel to $[\xi\xi 0]$, but individual atomic displacements need not be.

meV/atom) to that of $B2$ AlSc, which explains why the whole TA$[\bar{1}10]$ branch along $[\xi\xi 0]$ is so low in energy. The anomalous dispersion of the longitudinal $[\xi\xi\xi]$ phonon branch is characterized by a pronounced dip at 1/3[111]. The situation is reminiscent of the soft longitudinal 2/3$[\xi\xi\xi]$ phonon found in bcc transition metals displaying an instability with respect to the ω phase.[48,49] ω-like instabilities have been observed in ternary ordered $B2$ Ti-Al based alloys[50] and it is therefore interesting to note that the phonon dispersion curves in Fig. 5 suggest an incipient instability of the $B2$ phase in Al-Sc as well.

Figure 6 compares the calculated phonon DOS (solid lines) of cubic CsCl-type and orthorombic BCr-type AlSc

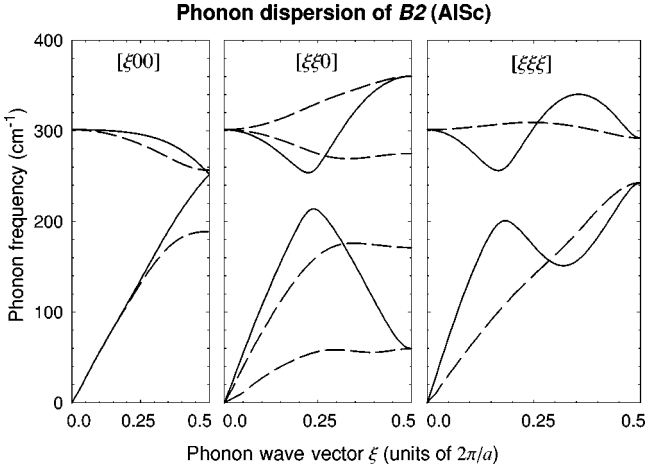

FIG. 5. Phonon dispersion curves of $B2$ AlSc. Solid lines show longitudinal modes while dashed lines show transversal phonon modes.

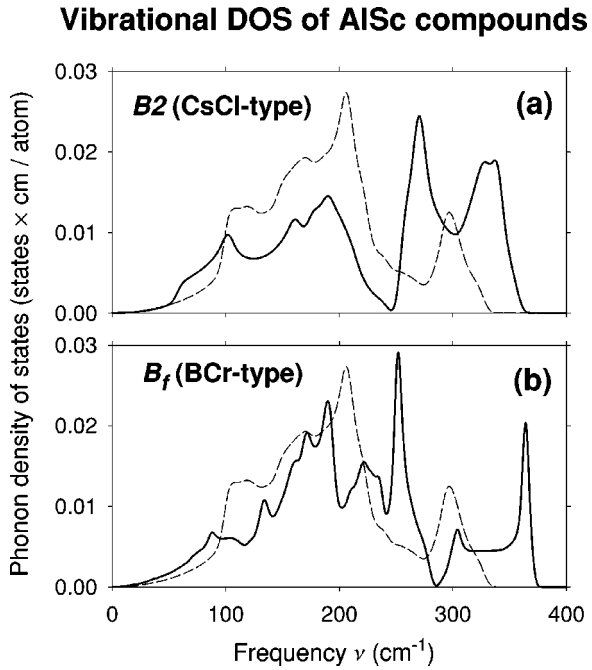

FIG. 6. Vibrational densities of states of (a) $B2$ AlSc and B_f AlSc compounds (solid lines). Dashed lines show composition-weighted vibrational DOS of hcp Sc and fcc Al.

compounds. The dashed line in Fig. 6 represents a composition-weighted average of the constituent phonon DOS of fcc Al and hcp Sc. In all cases, the difference between the vibrational DOS of ordered compounds and the composition-weighted average of the constituents [see the definition of $\Delta g(\omega)$ in Sec. II C] is negative in the low-frequency region below ≈ 220 cm^{-1}. In other words, the ordered compounds exhibit significantly higher phonon frequencies, indicative of a pronounced stiffening of interatomic bonds upon compound formation. This stiffening of the nearest-neighbor Al-Sc bonds is also manifested in higher values of the bulk moduli of Al_3Sc and AlSc compounds as compared to fcc Al and hcp Sc (see Table II). Since the logarithmic factor entering the formation entropy $\Delta S_{\rm vib}$ in Eq. (6) assigns more weight to the low-energy region of vibrational frequencies, negativity of $\Delta g(\omega)$ for low ω leads to large negative entropies of formation. The physical reasons for phonon stiffening upon compound formation in Al-Sc have been thoroughly discussed in Ref. 11, where it was shown that it is a manifestation of strong hybridization between electronic p orbitals of Al and d orbitals of Sc atoms, common to many transition-metal aluminide systems.[32,43,45]

It is also evident from Fig. 6 that the BCr-type structure has a higher phonon DOS than the cubic CsCl-type structure of AlSc in the intermediate-frequency range between 100 and 250 cm^{-1} and, thus, should also have a higher entropy. Indeed, the calculated value for the harmonic vibrational entropy difference between B_f and $B2$ phases of AlSc is $\Delta S_{\rm vib}^{B_f/B2} = +0.20 k_B$/atom. Using the $T=0$ K energy difference 0.07 meV/atom, we obtain that the BCr-type structure may be the stable phase of AlSc above $T=2460$ K (neglecting configurational contributions to the entropy). There are

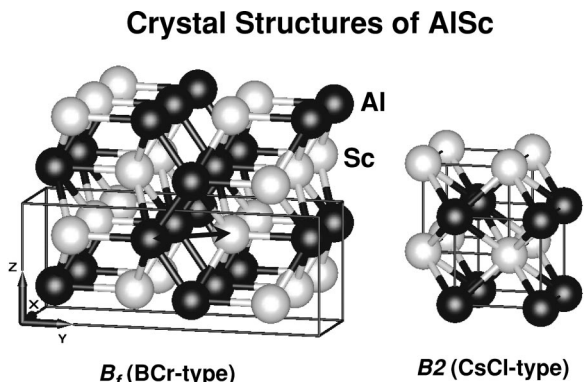

FIG. 7. Lattice structures of cubic $B2$ (CsCl-type) and orthorombic B_f (BCr-type) AlSc compounds. Al atoms are black and Sc atoms are gray. Directions of *x*, *y*, and *z* axes are perpendicular to the plane of the drawing, horizontal, and vertical, respectively.

some indications that the BCr-type structure is stable near the melting point, as has been observed in experiments of crystal growth from the liquid phase. However, the experimental situation is still not resolved, and further work is needed to settle the question. In this connection it is interesting to understand what the physical factors are contributing to the higher vibrational entropy of the BCr-type structure.

Figure 7 shows crystal structures of both AlSc compounds. In the cubic $B2$ structure each Al (Sc) atom has eight nearest-neighbor Sc (Al) atoms at a distance $d_{\text{Al-Sc}}=2.86$ Å. In contrast, in the orthorombic B_f structure each Sc atom has six nearest-neighbor Al atoms. Four of these Al atoms are at the same distance $d_{\text{Al-Sc}}=2.86$ Å as in the cubic $B2$ structure. The fifth Al-Sc bond is parallel to the *y* axis and is somewhat longer ($d_{\text{Al-Sc}}=2.91$ Å). Finally, the sixth Al atom is at a distance $d_{\text{Al-Sc}}=2.99$ Å. The former is indicated by an arrow but not shown as a bond in Fig. 7 since the corresponding force constant was found to be substantially weaker than those of the shorter Al-Sc bonds. Each Al atom in B_f has eight nearest neighbors: six Sc atoms and two Al atoms at a distance $d_{\text{Al-Al}}=2.61$ Å. Direct Al-Al bonds form zigzag chains along the *z* direction. It is interesting that these Al-Al bonds are very short, much shorter than Al-Al bonds in fcc Al (2.82 Å). Thus, it is reasonable to hypothesize that Al-Al bonds will be quite stiff and cause the local environment of Al atoms to be very anisotropic from a lattice dynamical point of view. Data presented in Table III show that this is indeed the case. We see that the root-mean-square (rms) vibrational displacements of Al atoms, $\sqrt{\langle u^2_{\text{Al},\alpha}\rangle}$, exhibit huge directional dependence: rms displacement along the *x* axis is twice larger than that along the *z* axis, with the *y* component being slightly higher than $\sqrt{\langle u^2_{\text{Al},z}\rangle}$, but much lower than $\sqrt{\langle u^2_{\text{Al},x}\rangle}$. In contrast, Sc displacements are much more isotropic. The largest rms displacements for Sc occur along the *z* axis and the smallest displacements occur along the *x* axis, but the difference is only 0.04 Å. Presumably, *z* is the hardest direction due to the considerable amount of Al-Sc bond stretching involved in Sc vibrations. Averages of the rms displacements over three Cartesian directions are slightly larger in B_f than in $B2$ for both Al (0.15 vs 0.14 Å) and Sc (0.14 vs 0.13 Å) atoms. Larger displacements generally mean softer interatomic forces, lower phonon frequencies, and higher vibrational entropies, which is manifested in the value $\Delta S^{B_f/B2}_{\text{vib}}=+0.20k_B$/atom quoted above.

TABLE III. Theoretically calculated vibrational properties of $B2$ and B_f phases of AlSc. We give the values of mean-square displacements $\sqrt{\langle u^2_{i\alpha}\rangle}$ at $T=600$ K, lowest-order moments of atom- and Cartesian direction-decomposed phonon DOS ($\overline{\ln \omega_{i\alpha}}$ and $\overline{\omega_{i\alpha}}$), and on-site restoring force constant $\Phi_{\alpha\alpha}(ii)=-\Sigma_j\Phi_{\alpha\alpha}(ij)$. Indices *i* and *j* number atoms in the crystal and α indexes Cartesian directions. Vibrational entropy difference between B_f and $B2$ is obtained by summing the partial logarithmic moments of DOS over all atoms and directions, $\Delta S^{B_f/B2}_{\text{vib}}=+0.40k_B$ per formula unit or $+0.2k_B$ per atom.

		$\sqrt{\langle u^2_{i\alpha}\rangle}$ at $T=600$ K (Å)	$-\overline{\ln \omega_{i\alpha}}$	$\overline{\omega_{i\alpha}}$ (cm^{-1})	$\Phi_{\alpha\alpha}(ii)$ (eV/Å^2)
B_f	Al(x)	0.22	−5.04	168	3.2
	Al(y)	0.13	−5.48	252	6.7
	Al(z)	0.11	−5.65	298	9.4
	Sc(x)	0.12	−5.18	185	6.1
	Sc(y)	0.14	−5.14	178	5.7
	Sc(z)	0.16	−5.12	182	6.1
$B2$	Al(x)	0.14	−5.43	247	6.8
	Sc(x)	0.13	−5.24	206	8.2

Another way to analyze vibrational properties of B_f and $B2$ compounds of AlSc is using atom- and direction-decomposed phonon DOS. The latter are defined as

$$\rho_{i\alpha}(\omega)=\frac{1}{N}\sum_{\mathbf{q}n}\delta(\omega-\omega_{\mathbf{q}n})|e_{i\alpha}(\mathbf{q}n)|^2, \tag{14}$$

where *i* numbers atoms in the unit cell, *N* is total number of atoms in the crystal, $\mathbf{q}$ is phonon wave vector, *n* runs over phonon branches, and $\mathbf{e}_i(\mathbf{q}n)$ are phonon mode eigenvectors. Figure 8 shows $\rho_{i\alpha}(\omega)$ in B_f for Al (upper panel) and Sc (lower panel) atoms. In accordance with the structural analysis of B_f AlSc (see above), partial phonon DOS in Fig. 8 shows a pronounced separation of Al vibrations along the *x*, *y*, and *z* axes, in order of increasing average frequency. In contrast, Sc partial DOS is distributed much more evenly among all three directions. The highest peak in phonon DOS of B_f at 370 cm^{-1} is due to Al vibrations along the ''elastically hard'' *z* axis, while the low-frequency region below 250 cm^{-1} involves almost exclusively Al(x) and Sc(x,y,z) vibrations. Table III gives the values of average partial frequencies $\omega_{i\alpha}$ [i.e., first moments of $\rho_{i\alpha}(\omega)$] and partial entropies [given by logarithmic moments of $\rho_{i\alpha}(\omega)$ taken with a minus sign]. We see that indeed the partial entropies $-\overline{\ln \omega_{i\alpha}}$ are highest for the softest directions. Summing over all directions for each kind of atom, we obtain that the partial vibrational entropy of Al is $0.12k_B$/atom higher in B_f than in

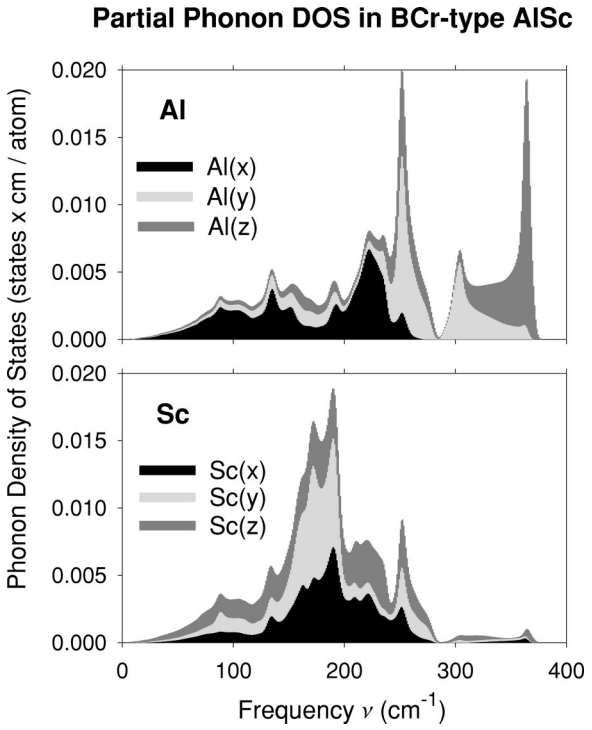

FIG. 8. Atom-decomposed partial phonon densities of states $\rho_{i\alpha}(\omega)$ for BCr-type AlSc, as defined in Eq. (14).

$B2$, and the partial entropy of Sc is $0.28k_B$/atom higher in B_f than in $B2$, leading to the total $\Delta S_{\rm vib}^{B_f/B2}=(0.12+0.28)/2=+0.20k_B$/atom.

In conclusion, the vibrational entropy is higher in the orthorombic B_f than in the more symmetric $B2$ structure of AlSc due to significant differences in local environments for both Al and Sc atoms, determined by the number, type, and stiffness of nearest-neighbor bonds. The effect of symmetry on the vibrational entropy of fcc-based alloys was noted already by van de Walle and Ceder.[51] These authors showed that structural symmetry has a pronounced effect on the length and stiffness of nearest-neighbor bonds in the Pd-V system, which was essential in explaining the surprising finding that the disordered alloy had a *lower* vibrational entropy than ordered Pd_3V. It is interesting that similar effect was recently found in another Al-based alloy: the well studied Al-Cu system. Wolverton and Ozoliņš[52] found that, contrary to many metallurgy textbooks, the tetragonal θ phase is not the most stable low-temperature phase of Al_2Cu. They showed that the more symmetric θ' phase of Al_2Cu has a lower energy, but the higher vibrational entropy of θ reverses the structural stability above $T_c\approx 500$ K. Higher vibrational entropy of the θ phase was traced back to the lower symmetry of this structure in comparison with the more symmetric θ', which allows certain low-frequency optical modes that involve little distortion of nearest-neighbor bond lengths. Thus, we hypothesize that the link between the degree of symmetry of a structure and its vibrational entropy is probably quite general and could be responsible for the occurence of some ''exotic'' low-symmetry intermetallic structures.

For the cubic $L1_2$ Al_3Sc and $B2$ AlSc structures we have

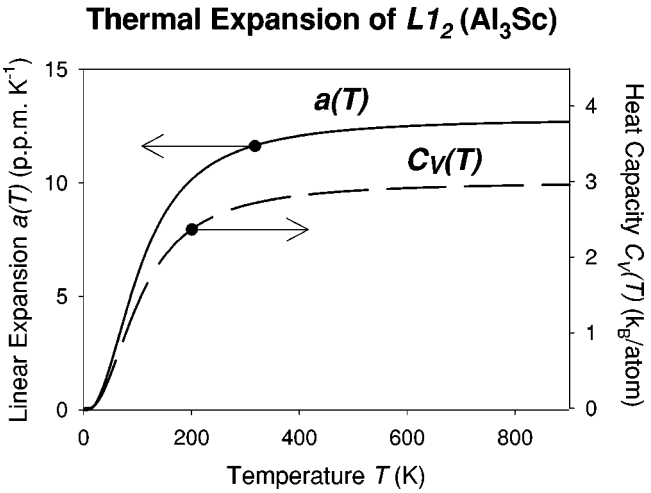

FIG. 9. Calculated coefficient of linear thermal expansion $\alpha_L(T)$ (solid line, left hand scale) and harmonic heat capacity $C_V(T)$ (dashed line, right hand scale) for cubic $L1_2$ Al_3Sc.

calculated the volume coefficients of thermal expansion (CTE), $\alpha_V=3\alpha_L$, and the temperature dependences of bulk moduli, as reported in Table II. We note that the CTE and bulk modulus results for the intermetallic compounds are significantly lower and higher, respectively, than expected from a composition-weighted average of the corresponding values for elemental Al and Sc. These results again reflect that Al-Sc compounds are significantly ''stiffer'' than the elemental constituents. For Al_3Sc a very recently measured value of the room-temperature CTE (Ref. 36) reported in Table II is even smaller than the first-principles calculated value, suggesting that the anharmonicity in the calculated equation of state for this intermetallic is overestimated. This result is interesting in light of the substantially better agreement between experiment and theory obtained for the elemental constituents (see Table II and Ref. 25). Some insight into this discrepancy may be gained by considering temperature dependence of $\alpha_L(T)$ in $L1_2$ Al_3Sc, shown in Fig. 9. According to Eq. (8), the coefficient of thermal expansion is proportional to the product of the Grüneisen parameter $\gamma(T)$ and constant-volume heat capacity $C_V(T)$. The latter shows a pronounced variation at and below the Debye temperature θ_D. As shown by a dashed line in Fig. 9, the harmonic heat capacity of cubic Al_3Sc exhibits considerable variation even at T as high as $T=300$ K, where it has reached only 88% of its Dulong-Petit limit $3k_B$. This indicates that the Debye temperature of Al_3Sc is unusually high and, therefore, the temperature dependence of thermal expansion cannot be neglected. Indeed, it is evident from Fig. 9 that, just like the heat capacity $C_V(T)$, at $T=300$ K the coefficient of linear thermal expansion $\alpha_L(T)$ has reached only 88% of its high-T limit.

C. Free energy models and solvus boundaries for Al-rich alloys

The location of the Al-rich solvus boundary (i.e., the Al side of the two-phase boundary between the Al solid solution and the ordered Al_3Sc phase) is of primary importance in the

TABLE IV. Sc impurity electronic free energies (G_{el}), enthalpies (H_{el}), and entropies (S_{el}) calculated as a function of electronic temperature. Results are given for different supercell sizes and number of reciprocal space **k** points employed in the electronic-structure calculations. The number of equivalent **k** points (Ref. 21) refers to a primitive (one-atom) fcc unit cell. Impurity thermodynamic properties are expressed in terms of a difference involving formation quantities for the Al_3Sc phase (α'), as discussed in the text.

Supercell	k_BT (eV)	**k** Points	$4\Delta G_{el}^{\alpha'}-\Delta G_{el}^{Sc}$ (eV)	$4\Delta H_{el}^{\alpha'}-\Delta H_{el}^{Sc}$ (eV)	$4\Delta S_{el}^{\alpha'}-\Delta S_{el}^{Sc}$ (k_B)
64	0.08	182	−0.769	−0.798	−0.366
64	0.08	408	−0.767	−0.790	−0.281
64	0.08	770	−0.788	−0.830	−0.525
64	0.08	1300	−0.769	−0.789	−0.257
128	0.08	182	−0.825	−0.850	−0.309
216	0.08	182	−0.788	−0.811	−0.291
216	0.06	182	−0.796	−0.827	−0.391
216	0.04	182	−0.811	−0.853	−0.522

processing of two-phase Al/Al_3Sc alloys. In Fig. 1 of our previous paper,[11] first-principles phase boundaries calculated with different levels of approximation were plotted and compared with experimentally measured solubility data.[53–56] In this section we discuss these results in further detail.

In order to calculate the solvus boundary, the free energies of both the Al solid solution phase (to be denoted as α below) as well as the Al_3Sc intermetallic compound (denoted here as α') are required as functions of composition and temperature. In previous first-principles studies[30,11] it was found that with very high accuracy the free energies of the α and α' phases can be modeled as an ideal solution (corresponding to a solid solution of noninteracting Sc substitutional impurities) and a stoichiometric line compound, respectively. For the α phase the accuracy of the ideal solution model reflects the very dilute (less than 0.2 at. %) concentrations of Sc which can be accomodated in solution under equilibrium conditions. Furthermore, the line-compound approximation for the α' phase is consistent with the high-temperature x-ray-scattering measurements of Sparks *et al.*[57] who found that Al_3Sc remains nearly perfectly ordered up to its melting point. This approximation is further consistent with atom-probe/field-ion microscopy measurements by Sano *et al.*[58] who report that Al_3Sc precipitates in annealed Al 0.19 at. % Sc alloys are very nearly stoichiometric.

Within the ideal-solution approximation, the zero-pressure Gibbs free energy of formation ΔG^{α} for the Al solid-solution phase can be written as follows (expressed per atom):

$$\Delta G_{\alpha}(T,x)=\Delta G^{Sc}(T)x+k_BT[x\ln x+(1-x)\ln(1-x)], \tag{15}$$

where x is the atomic fraction of Sc and k_B is Boltzmann's constant. $\Delta G^{Sc}(T)$ in Eq. (15) denotes the temperature-dependent free energy of formation of a single Sc substitutional impurity in fcc Al. Within the line-compound approximation discussed above, the zero-pressure formation free energy of the Al_3Sc phase, $\Delta G^{\alpha'}(T)$ (again expressed per atom), depends only upon T.

In calculating the solvus boundaries shown in Fig. 1 of Ref. 11 we neglected possible coherency effects, modeling the phase boundaries as corresponding to incoherent phase equilibria between the α and α' phases. Employing the usual common-tangent construction combined with the ideal-solution and line-compound approximations, the temperature-dependent solubility limit x_s of Sc in Al can be written as follows:

$$x_s(T)=\exp\left[\frac{4\Delta G^{\alpha'}(T)-\Delta G^{Sc}(T)}{k_BT}\right], \tag{16}$$

where the factor of 4 in front of $\Delta G^{\alpha'}$ originates from the stoichiometry of the Al_3Sc phase. The free energies entering Eq. (16) were calculated from first principles including electronic and vibrational contributions as described in Sec. II.

While the precise calculation of electronic free energies for the intermetallic Al_3Sc compound is straightforward, deriving well-converged values for the Sc impurity is significantly more difficult. In the impurity calculations use has been made of supercell approaches as reviewed for calculations of point defects in Al by Chetty *et al.*[59] and Turner *et al.*[60] As has been demonstrated by these authors, the accurate calculation of dilute impurity energies in Al based upon such methods often requires relatively large supercells and dense meshes of reciprocal-space **k**-points. In Table IV we show the dependence of the computed values of $4\Delta G^{\alpha'}-\Delta G^{Sc}$ [see Eq. (16)] upon supercell size and number of **k** points employed in the electronic-structure calculations. For all of the calculations listed in Table IV use was made of VASP (as detailed above) and "equivalent" **k** point[21] sets corresponding to 182, 408, 770, and 1300 irreducible **k** points for primitive (one atom per cell) fcc Al. For calculating ΔG^{Sc}, use was made of 64-, 128-, and 216-atom supercells in which the Sc impurities are separated by 4, 4.899, and 6 nearest-neighbor spacings, respectively. From the results listed in the top six lines of Table IV the calculated electronic free energies are found to vary with supercell size and **k** points on the order of 0.02–0.04 eV. Due to the exponential dependence of the solubility limits upon these free energies, such variations give rise to 30–40 % uncertainties in calculated solubility limits at a representative temperature of 930

K ($k_BT=0.08$ eV). Such uncertainties in the calculated solubility translate into 40–50 K uncertainties in the solvus boundary at the maximum solubility limit.

In the results given in Fig. 1 of Ref. 11 use was made of free energies derived from the 216-atom supercells. The last three lines in Table IV give the caculated values of the electronic impurity free energies as a function of the electronic temperature, ranging between $k_BT=0.04$ and 0.08 eV (T ranging between 465 and 930 K). These results were fit to a polynomial of the form given in Eq. (4) for the purpose of calculating the temperature-dependent solubility limits shown in Fig. 1 of Ref. 11. The dot-dashed line in Fig. 1 of Ref. 11 gives the resulting calculated solubility limits based upon the electronic contributions to the free energies entering Eq. (16). By comparison, the dotted line in Fig. 1 of Ref. 11 corresponds to calculated solubility limits derived from zero-temperature energies alone. The latter calculations overestimate the temperature scale relative to experimental data by roughly 600 K at the maximum measured solubility concentration of 0.2 at. % Sc. A comparison of the dotted and dot-dashed curves shows that the effect of finite-temperature electronic excitations (electronic entropy) is an appreciable (roughly 100 K) reduction in the calculated solvus boundaries. This effect reflects the larger electronic free energy, per atom, of the Sc atoms in Al relative to the Al_3Sc compound.

The lower two curves in Fig. 1 of Ref. 11 correspond to calculated solubility limits derived by combining the electronic free energies with calculated values of the vibrational entropy as discussed previously.[11] Harmonic vibrational free energies for the Sc impurity were derived from linear-response calculations of dynamical matrices for 27-atom supercells (the variation in calculated impurity vibrational entropies with system size is discussed in Ref. 11). The solid line in Fig. 1 of Ref. 11 corresponds to calculated solubility limits derived by including electronic and harmonic vibrational free energy contributions to ΔG^{Sc} and $\Delta G^{\alpha'}$ in Eq. (16). Harmonic vibrations give rise to an entropic contribution to the free energies which is constant at high temperatures. As a result, the harmonic vibrational entropy leads to a constant prefactor in Eq. (16). Our calculated vibrational-entropy prefactor results in a factor of 27 increase in the calculated solubility limits shown in Fig. 1 of Ref. 11. From a comparison of the solid and dashed-dotted lines in this figure, the effect of harmonic vibrational entropy is seen to be a 450 K decrease in the calculated solvus boundary temperature at 0.2 at. % Sc.

Due to the high homologous temperatures involved in Fig. 1 of Ref. 11 it is expected that anharmonic effects may lead to non-negligible corrections to the vibrational free energies. We have estimated the importance of anharmonic terms based upon the quasiharmonic approximation[24] as described in Sec. II. The calculated effect on the solubility is plotted with a dashed line in Fig. 1 of Ref. 11. Anharmonic effects, incorporated through the quasiharmonic approximation, are seen to result in a relatively small ($\approx 20\%$) shift in the solubility limits at the highest temperatures. It is interesting to note that thermal expansion acts to slightly *reduce* the vibrational entropy difference $\Delta S^{\mathrm{vib}}_{\mathrm{Sc}} - 4\Delta S^{\mathrm{vib}}_{\alpha'}$. This is somewhat counterintuitive, since Al_3Sc is much stiffer (higher bulk modulus) than fcc Al, has a low Grüneisen parameter, and thus expands very little in comparison with Al. The apparent contradiction can be explained by considering the change in Grüneisen parameter γ_G with respect to fcc Al and evaluated per Sc atom. This quantity is larger for the Sc impurity ($\Delta\gamma_G=-3.2$) than for ordered Al_3Sc ($\Delta\gamma_G=-2.1$). It is possible, however, that the magnitude of the anharmonic contributions to the Sc impurity free energy is underestimated in the quasiharmonic approximation. Detailed comparisons between between Monte Carlo and quasiharmonic results were performed for bulk and defect free energies in Cu by Foiles.[26] It was found that, while bulk free energies are accurately described by the quasiharmonic approximation to very high homologous temperatures, anharmonic contributions to point-defect free energies were significantly underestimated. We note that larger anharmonic contributions to the Sc impurity free energy would have the effect of moving the dashed line in Fig. 1 of Ref. 11 to the right, potentially improving even further the agreement with experimental solubility data.

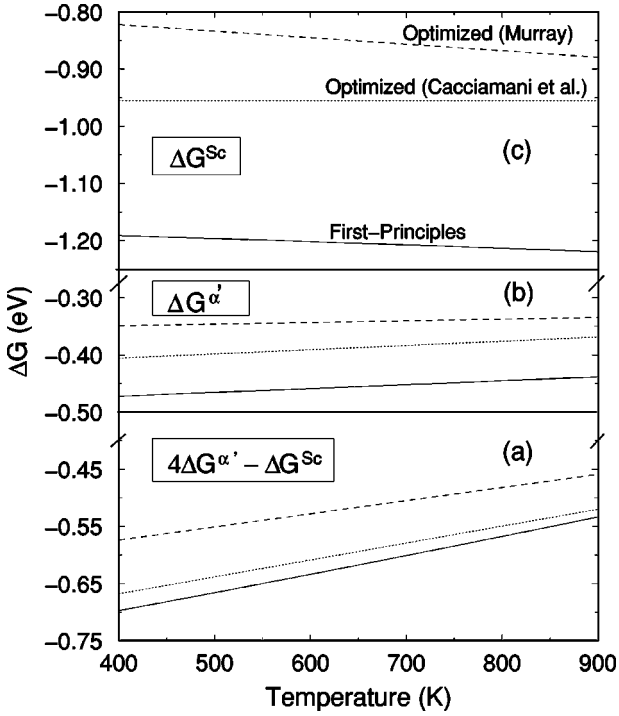

FIG. 10. Temperature dependent values of ΔG^{Sc} (top panel), $\Delta G^{\alpha'}$ (middle panel), and $4\Delta G^{\alpha'} - \Delta G^{\mathrm{Sc}}$. Solid lines are first-principles results, while dashed and dotted lines are derived from the optimized thermodynamic parameters due to Murray (Ref. 3) and Cacciamani *et al.* (Ref. 4), respectively.

In Fig. 10 the solid lines represent the first-principles values of the thermodynamic functions entering Eq. (16) (including all electronic and vibrational contributions), with ΔG^{Sc}, $\Delta G^{\alpha'}$, and $4\Delta G^{\alpha'} - \Delta G^{\mathrm{Sc}}$ plotted in the top (c), middle (b), and bottom (a) panels, respectively. The dashed and dotted lines are from optimized thermodynamic models derived in recent phase diagram assessments,[3,4] and will be discussed below. Due to the negative formation entropy of

the ordered Al_3Sc phase (see Fig. 2), the formation free energy $\Delta G^{\alpha'}$ (plotted in the middle panel) increases with temperature by roughly 0.03 eV between 400 and 900 K. The temperature dependence of the calculated Sc impurity free energy (top panel) is of comparable magnitude, but shows the *opposite sign*. The temperature dependence of $\Delta G^{\alpha'}$ and ΔG^{Sc} is seen to be very well approximated as linear in Figs. 10(b) and 10(c), indicating that the largest contribution to the temperature dependence of these free energies originates from harmonic vibrational entropy.

The large effect of nonconfigurational free energy upon the calculated solvus boundary demonstrated in Fig. 1 of Ref. 11 is associated with the temperature dependence of the quantity $4\Delta G^{\alpha'}-\Delta G^{\mathrm{Sc}}$, which is seen to decrease in magnitude by 0.16 eV between 400 and 900 K in Fig. 10(a). From the results in the top two panels of this figure, it is seen that this temperature dependence results primarily from the large negative formation entropy of the Al_3Sc ordered compound, coupled with the positive excess entropy per Sc impurity in Al. The large magnitude of ΔS for the Al_3Sc compound is due primarily to harmonic vibrational entropy. Whereas this contribution is large and *negative* $(-0.7k_B/\mathrm{atom})$ for the compound, we find that the corresponding value for the Sc impurity is smaller and *positive* $(+0.36k_B/\mathrm{atom}-0.50k_B/\mathrm{atom})$.[11] The microscopic origin of this nonintuitive result is discussed in detail by Ozoliņš and Asta.[11]

D. Comparison of first-principles and assessed thermodynamic models

In Figs. 1, 2, and 10 our first-principles calculated thermodynamic properties are compared with values obtained using optimized thermodynamic parameters developed in recent phase-diagram assessments by Murray[3] and Cacciamani *et al.*[4] In both of these assessments the Al solid-solution phase was modeled as a regular solution, with a mixing free energy of the following form (again expressed per atom):

$$\begin{aligned}\Delta G_\alpha(T,N,x) &= A^\alpha(T)x(1-x)+k_BT[x\ln x \\ &\quad +(1-x)\ln(1-x)] \\ &\approx A^\alpha(T)x+k_BT[x\ln x \\ &\quad +(1-x)\ln(1-x)]. \end{aligned} \tag{17}$$

The second expression on the right-hand side of Eq. (17) is highly accurate for the dilute compositions shown in Fig. 1 of Ref. 11, and the parameter A^α therefore can be equated with the Sc impurity free energy ΔG^{Sc} in Eq. (15). As in the present first-principles calculations, Murray and Cacciamani *et al.* modeled the free energy of the Al_3Sc phase as a line compound.

In Fig. 10 we plot with dashed and dotted lines the thermodynamic functions ΔG^{Sc}, $\Delta G^{\alpha'}$, and $4\Delta G^{\alpha'}-\Delta G^{\mathrm{Sc}}$ derived from the optimized thermodynamic parameters of Murray and Cacciamani *et al.*, respectively. The latter values are seen to be somewhat closer to the present calculated results, especially for the free energy difference related to the solubility limits, $4\Delta G^{\alpha'}-\Delta G^{\mathrm{Sc}}$. The parameters of Cacciamani *et al.* are also seen to give rise to better agreement with experimental measurements, and the present first-principles results, for the enthalpy and entropy of formation for the Al_3Sc compound in Figs. 1 and 2. This improved agreement can be attributed to the fact that the calorimetry measurements of formation enthalpies were incorporated into the thermodynamic optimization by Cacciamani *et al.* while they were not by Murray.

On the basis of the comparisons discussed above, the thermodynamic models of Cacciamani *et al.* seem to reproduce well available experimental data, as well as the important features of the present first-principles results. By contrast, the Murray parameters appear to underestimate the magnitudes of both the entropy and enthalpies of formation for Al-rich alloys. This observation is interesting in light of previous work which used the Murray thermodynamic functions as a basis for modeling Al_3Sc precipitation kinetics in supersaturated Al(Sc) alloys.[2,61] The Murray numbers lead to significantly smaller thermodynamic driving forces for the nucleation of Al_3Sc precipitates relative to the predictions of both the models of Caccimani *et al.* and our first-principles results. In light of this result, a reanalysis of the nucleation data[2] based upon the thermodynamic parameters of Cacciamani *et al.* would be of interest.

IV. DISCUSSION

The dashed and solid lines in Fig. 1 of Ref. 11 demonstrate a large effect of ionic vibrational free energy upon the calculated solubility limits. It is interesting to note that the important role of vibrational free energy in dictating solid solubility limits was suggested already 50 years ago by Zener.[62] Zener used an expression formally equivalent to Eq. (16) to analyze the temperature dependences of measured solubility limits for Ni, Mn, Cr, Si, Cu, and Zr in Al,[63] assuming that the enthalpy and entropy are independent of temperature:

$$x_s(T)=\exp\left(\frac{\Delta S}{k_B}\right)\exp\left(\frac{-\Delta H}{k_BT}\right). \tag{18}$$

By plotting the logarithm of x_s versus $1/T$, Zener showed that the measured data fall approximately on a straight line with intercepts at $1/T=0$ corresponding to $\Delta S/k_B$ in Eq. (18). Values of the factor $\exp(\Delta S/k_B)$ so obtained by Zener ranged from 10, for zirconium, to 60, for nickel. The factor of 27 increase in calculated solubility limits due to the vibrational entropy, obtained in the present work, falls in the middle of this range of values found by Zener.

More recently, the important role of vibrational free energy in the calculations of alloy phase diagrams has been suggested by Anthony and co-workers.[64–67] Specifically, these authors have employed a variety of experimental techniques, including neutron scattering, calorimetry, and electron-energy-loss spectroscopy, to measure vibrational entropy differences between ordered and disordered phases of Ni_3Al, Cu_3Au, and Fe_3Al. These measurements give rise to values of ΔS^{vib} ranging between $(0.14\pm0.05)k_B/\mathrm{atom}$ for

Cu_3Au,[66] (0.2–0.3)k_B/atom in Ni_3Al,[64,65] and (0.10 $\pm$0.03)k_B/atom in Fe_3Al.[67] Based upon these values, which represent substantial fractions of the maximum configurational entropy difference ($0.57k_B$/atom) between ordered and disordered phases at an A_3B composition, it has been concluded that vibrational entropy may have large effects upon calculated order-disorder transition temperatures in substitutional alloys. However, in first-principles theoretical studies investigating the configurational dependence of the vibrational entropy,[68,69,51] relatively small effects have been obtained. For Ni_3Al, van de Walle, Ceder, and Waghmare[68] obtained a negligible entropy difference between fully ordered and disordered phases. For Pd_3V, van de Walle and Ceder[51] recently obtained $\Delta S^{\mathrm{vib}} = -0.07k_B$/atom; i.e., the disordered state was found to have a *lower* vibrational entropy than the ordered $D0_{22}$ compound. For Cu_3Au, Ozoliņš, Wolverton, and Zunger[69] calculated a value of $\Delta S^{\mathrm{vib}} = 0.08k_B$/atom. The net effect of vibrational contributions to the free energy upon the order-disorder transtion temperature was calculated to be roughly 14% (75 K).[69] The current results point to a much more substantial effect of vibrational entropy upon calculated temperatures for phase boundaries between substitutional alloy phases with *differing compositions*. Clearly, further work on other alloy systems is warranted to assess the generality of our findings for Al-rich Al-Sc alloys. However, the results of the analysis by Zener[62] suggest that vibrational entropy may lead to significant reductions in the temperature scales of calculated phase boundaries in a wide range of Al-based alloys.

ACKNOWLEDGMENTS

We gratefully acknowledge Dr. R. W. Hyland, Jr., for many helpful discussions and suggestions. We also thank Professor D. N. Seidman for pointing out Ref. 62 and Dr. G. Cacciamani for providing unpublished thermodynamic parameters. Research at Northwestern was supported by the National Science Foundation under program DMR-0080766. Research at Sandia was supported by the U.S. Department of Energy, Office of Basic Energy Sciences, Materials Science Division, under Contract No. DE-AC04-94AL85000. This research used resources of the National Energy Research Scientific Computing Center, which is supported by the Office of Science of the U.S. Department of Energy under Contract No. DE-AC03-76SF00098.

[1] M. E. Drits, L. S. Toropova, R. L. Gushchina, and S. G. Fedotov, J. Sov. Non Ferrous Met. Res. **12**, 83 (1984).
[2] R. W. Hyland, Jr., Metall. Trans. A **23**, 1947 (1992).
[3] J. L. Murray, J. Phase Equilib. **19**, 380 (1998).
[4] G. Cacciamani, P. Riani, G. Borzone, N. Parodi, A. Saccone, R. Ferro, A. Pisch, and R. Schmid-Fetzer, Intermetallics **7**, 101 (1999).
[5] J. C. Schuster and J. Bauer, J. Less-Common Met. **109**, 345 (1985).
[6] O. Schob and E. Parthé, Acta Crystallogr. **19**, 214 (1965).
[7] D. de Fontaine, Solid State Phys. **47**, 33 (1994).
[8] F. Ducastelle, *Order and Phase Stability in Alloys* (North-Holland, New York, 1991).
[9] A. Zunger, in *Statics and Dynamics of Alloy Phase Transformations*, edited by P. E. A. Turchi and A. Gonis, Vol. 319 of *NATO Advanced Study Institute, Series B: Physics* (Plenum, New York, 1994).
[10] U. R. Kattner, JOM **49**, 14 (1997).
[11] V. Ozoliņš and M. Asta, Phys. Rev. Lett. **86**, 448 (2001).
[12] S. Baroni, P. Giannozzi, and A. Testa, Phys. Rev. Lett. **58**, 1861 (1987); P. Giannozzi, S. de Gironcoli, P. Pavone, and S. Baroni, Phys. Rev. B **43**, 7231 (1991).
[13] J. P. Perdew and A. Zunger, Phys. Rev. B **23**, 5048 (1981).
[14] G. Kresse and J. Hafner, Phys. Rev. B **47**, 558 (1993); **49**, 14 251 (1994).
[15] G. Kresse and J. Furthmüller, Comput. Mater. Sci. **6**, 15 (1996).
[16] G. Kresse and J. Furthmüller, Phys. Rev. B **54**, 11 169 (1996).
[17] D. Vanderbilt, Phys. Rev. B **41**, 7892 (1990).
[18] H. J. Monkhorst and J. D. Pack, Phys. Rev. B **13**, 5188 (1976); **16**, 1748 (1977).
[19] A. M. Rappe, K. M. Rabe, E. Kaxiras, and J. D. Joannopoulos, Phys. Rev. B **41**, 1227 (1990).
[20] S. G. Louie, S. Froyen, and M. L. Cohen, Phys. Rev. B **26**, 1738 (1982).
[21] S. Froyen, Phys. Rev. B **39**, 3168 (1989).
[22] Z. W. Lu, S.-H. Wei, A. Zunger, S. Frota-Pessoa, and L. G. Ferreira, Phys. Rev. B **44**, 512 (1991).
[23] G. Grimvall, *Thermophysical Properties of Materials* (North-Holland, Amsterdam, 1999).
[24] A. A. Maradudin, E. W. Montroll, and G. H. Weiss, *Theory of Lattice Dynamics in the Harmonic Approximation* (Academic Press, New York, 1963).
[25] A. A. Quong and A. Y. Liu, Phys. Rev. B **56**, 7767 (1997).
[26] S. M. Foiles, Phys. Rev. B **49**, 14 930 (1994).
[27] *Pearson's Handbook of Crystallographic Data for Intermetallic Phases*, 2nd ed., edited by P. Villars and L. D. Calvert (ASM International, Materials Park, OH, 1991), p. 999.
[28] R. W. Hyland, Jr. and R. C. Stiffler, Scr. Metall. Mater. **25**, 473 (1991).
[29] E. P. George, J. A. Horton, W. D. Porter, and J. H. Schneibel, J. Mater. Res. **5**, 1639 (1990).
[30] M. Asta, S. M. Foiles, and A. A. Quong, Phys. Rev. B **57**, 11 265 (1998).
[31] C. L. Fu, J. Mater. Res. **5**, 971 (1990).
[32] J.-H. Xu and A. J. Freeman, Phys. Rev. B **41**, 12 553 (1990).
[33] O. K. Anderson, Phys. Rev. B **12**, 3060 (1975); D. R. Hamman, Phys. Rev. Lett. **42**, 662 (1979); E. Wimmer, H. Krakauer, M. Weinert, and A. J. Freeman, Phys. Rev. B **24**, 864 (1981); S.-H. Wei and H. Krakauer, Phys. Rev. Lett. **55**, 1200 (1985); S.-H. Wei, H. Krakauer, and M. Weinert, Phys. Rev. B **32**, 7792 (1985).
[34] *American Institute of Physics Handbook*, edited by D. E. Gray (McGraw-Hill, New York, 1972); *Thermal Expansion*, edited by

Y. S. Touloukian *et al.* (Plenum, New York, 1975).
[35] C. Kittel, *Introduction to Solid State Physics* (Wiley, New York, 1986).
[36] Y. Harada and D. C. Dunand (unpublished).
[37] W.-G. Jung, O. J. Kleppa, and L. Topor, J. Alloys Compd. **176**, 309 (1991).
[38] S. V. Meschel and O. J. Kleppa, in *Metallic Alloys: Experimental and Theoretical Perspectives*, edited by J.S. Faulkner and R. G. Jordan, Vol. 256 of *NATO Advanced Study Institute, Series E: Applied Sciences* (Plenum, New York, 1994), p. 103.
[39] In comparing our calculated values of ΔH with experimental measurements we have not considered the values obtained by Pyagai and Vakhobov [I. N. Pyagai and A. V. Vakhobov, Russ. Metall. **15**, 50 (1990)] from acid solution calorimetry. As discussed by Cacciamani *et al.* (Ref. 4), the Pyagai-Vakhobov data appear too negative in comparison with other data for this and related systems.
[40] M. Alatalo, M. Weinert, and R. E. Watson, Phys. Rev. B **57**, R2009 (1998).
[41] M. Asta, D. de Fontaine, and M. van Schilfgaarde, J. Mater. Res. **8**, 2554 (1993).
[42] R. E. Watson and M. Weinert, Phys. Rev. B **58**, 5981 (1998).
[43] A. Carlsson and P. J. Meschter, J. Mater. Res. **4**, 1060 (1989).
[44] D. Nguyen-Manh and D. G. Pettifor, Intermetallics **7**, 1095 (1999).
[45] M. Weinert and R. E. Watson, Phys. Rev. B **58**, 9732 (1998).
[46] I. C. Bain, Trans. AIME **70**, 25 (1924).
[47] W. G. Burgers, Physica (Amsterdam) **1**, 561 (1934); also A. Nagasawa, N. Nakanishi, and K. Enami, Philos. Mag. A **43**, 1345 (1981).
[48] K.-M. Ho, C. L. Fu, B. N. Harmon, W. Weber, and D. R. Hamann, Phys. Rev. Lett. **49**, 673 (1982).
[49] K.-M. Ho, C. L. Fu, and B. N. Harmon, Phys. Rev. B **29**, 1575 (1984).
[50] L. A. Benderksy, W. J. Boettinger, B. P. Burton, and F. S. Biancaniello, Acta Metall. Mater. **38**, 931 (1990).
[51] A. van de Walle and G. Ceder, Phys. Rev. B **61**, 5972 (2000).
[52] C. Wolverton and V. Ozoliņš, Phys. Rev. Lett. **86**, 5518 (2000).
[53] S. Fujikawa, M. Sugaya, H. Takei, and K. Hirano, J. Less-Common Met. **63**, 87 (1979).
[54] H.-h. Jo and S. I. Fujikawa, Mater. Sci. Eng., A **171**, 151 (1993).
[55] M. E. Drits, E. S. Kadaner, T. V. Dobatkina, and N. I. Turkina, Russ. Metall. **4**, 152 (1973).
[56] L. A. Wiley (unpublished), cited in Ref. 3.
[57] C. J. Sparks, E. D. Specht, G. E. Ice, P. Zschack, and J. Schneibel, in *High Temperature Ordered Intermetallic Alloys IV*, edited by L. Johnson, D. P. Pope, and J. O. Stiegler, Mater. Res. Soc. Symp. Proc. **213** (MRS, Pittsburgh, 1991), p. 363.
[58] N. Sano, Y. Hasegawa, K. Hono, H. Jo, H. W. Pickering, and T. Sakurai, J. Phys. (Paris), Colloq. **11**, C6-337 (1987).
[59] N. Chetty, M. Weinert, T. S. Rahman, and J. W. Davenport, Phys. Rev. B **52**, 6313 (1995).
[60] D. E. Turner, Z. Z. Zhu, C. T. Chan, and K. M. Ho, Phys. Rev. B **55**, 13 842 (1997).
[61] C. L. Rohrer, M. Asta, S. M. Foiles, and R. W. Hyland, Jr., in *Thermodynamics and Kinetics of Phase Transformations*, edited by J. S. Im, B. Park, A. L. Greer, and G. B. Stephenson, Mater. Res. Soc. Symp. Proc. **398** (MRS, Pittsburgh, 1996), p. 477.
[62] C. Zener, in *Thermodynamics in Physical Metallurgy*, edited by C. Zener (ASM, Cleveland OH, 1950), p. 16–27.
[63] W. L. Fink and H. R. Freche, Trans. Am. Inst. Min., Metall. Pet. Eng. **111**, 304 (1934).
[64] L. Anthony, J. K. Okamoto, and B. Fultz, Phys. Rev. Lett. **70**, 1128 (1993).
[65] B. Fultz, L. Anthony, L. J. Nagel, R. M. Nicklow, and S. Spooner, Phys. Rev. B **52**, 3315 (1995).
[66] L. J. Nagel, L. Anthony, and B. Fultz, Philos. Mag. Lett. **72**, 421 (1995).
[67] L. Anthony, L. J. Nagel, J. K. Okamoto, and B. Fultz, Phys. Rev. Lett. **73**, 3034 (1994).
[68] A. van de Walle, G. Ceder, and U. V. Waghmare, Phys. Rev. Lett. **80**, 4911 (1998).
[69] V. Ozoliņš, C. Wolverton, and A. Zunger, Phys. Rev. B **58**, R5897 (1998).